Paper presented at the
75th SEG Conference & Exhibition
Houston, USA, 6th -11th November 2005

A two-step approach to depth migration of low frequency electromagnetic data

Written by R. Mittet, Frank Maaø, Odd M. Aakervik and Svein Ellingsrud

Presented by R. Mittet

emgs

ELECTROMAGNETIC GEOSERVICES AS

A two-step approach to depth migration of low frequency electromagnetic data.

Rune Mittet, Frank Maaø, Odd M. Aakervik and Svein Ellingsrud, EMGS

Summary

In order to migrate electromagnetic data from a low frequency controlled source, 3D electromagnetic Green functions should be used since the near-field effects may be large. Imaging principles of the correlation type do not have sufficient depth sensitivity to be used in a one-pass migration step. Depth sensitivity is increased if a non-local operator is introduced in the imaging condition. This operator accounts for the lateral propagation of the EM field in the high resistivity reservoir. The non-local operator depends on two parameters related to the resistivity and thickness of an assumed resistivity anomaly. These parameters can be estimated from a limited set of forward modeling operations.

Introduction

The Sea Bed Logging (SBL) method is described by Eidesmo et al. (2002). The main idea is to use an active source to probe the underground for thin, high resistive, layers. Hydrocarbon filled reservoirs will typically have a resistivity that is one to two orders of magnitude higher than a water filled reservoir. It will also have a resistivity that is one to two orders of magnitude higher than the surrounding shale or mudrock, and this is sufficient to support a partially guided wave in the reservoir that will leak energy up to receivers placed on the sea bed. The actual experiment is performed by dropping electric and magnetic sensors on the sea bed along a predetermined sail line and thereafter towing a horizontal electric dipole source along the line. The sail line starts at approximately 10 km before the first receiver and ends at approximately 10 km after the last receiver. Thus, all receivers have at least active source data with source receiver offsets of 10 km. The experimental geometry is similar to that of sea bed seismic data acquisition. It is well known that wave equation prestack depth migration of sea bed seismic data may be successful, given a good migration velocity model. Depth migration of sea bed EM data in a similar fashion is possible if the elastic wave equation is replaced by the Maxwell equations. However, additional problems must be addressed in depth migration of EM data.

First, the intermediate and high offset electromagnetic response from a hydrocarbon reservoir is not dominantly a reflection. This can be seen from the linear phase increase with offset of this event. The electromagnetic field excited in the reservoir behaves as a partially guided wave, propagating laterally through the reservoir and leaking energy back towards the receivers. The phase behavior as a function of offset is as for a refracted wave. Thus, Claerbouts imaging principle, which amounts to a correlation of up and down going energy in each subsurface location, is not ideal for imaging of hydrocarbon reservoirs with EM data.

Second, absorption and dispersion effects are much larger in EM data than in seismic data. Therefore, only low frequencies are available for imaging. Compensation for absorption and dispersion can in principle be done in the PSDM step for seismic data (Mittet et al., 1995). For EM data, stability becomes a problem if absorption compensation is applied in depth migration.

Third, the phase behavior of the electromagnetic field must be respected. In the far-field the electromagnetic field behaves as a "seismic wave" where phase increase linearly with propagation distance if the velocity is locally constant, however, for a typical overburden formation (1 Ωm to 3 Ωm) and typical frequencies (0.25 Hz to 2 Hz) the near-field may reach several kilometers into the formation. For the near-field of a horizontal electric dipole in a conducting medium, the phase does not necessarily increase linearly with propagation distance even if the velocity is constant. The near-field is of course causal but appear to be nearly instantaneous for example in the depth direction. It is only in the far-field that the propagation velocity or phase gradient approaches that of a locally plane electromagnetic wave. To get the correct phase behavior of the fields, the Maxwell equations must be solved in 3D. In seismic depth migration of line data, a 2D scheme can be used with success, since the phase of the 2D Green function is very close to the phase of the 3D Green function, except for a constant shift which is nearly independent of source receiver offset. For EM migration this is not the case since the phase of the 2D Green function differs everywhere from the phase of the 3D Green function.

Tompkins (2004) reported migration of EM data using 1D propagators and Claerbouts imaging principle. The migration scheme discussed in the following differ significantly from that approach. We recognize that Claerbouts imaging principle is not directly applicable and that the imaging principle should be modified to account for the partially guided wave in the reservoir. We do migration with full electromagnetic 3D Green functions that are calculated with a finite difference algorithm which solve for generally inhomogeneous media and also anisotropy if desired.

Theory

In Mittet et al. (1994), the elastic outgoing energy flux density of the misfit field was used as an error functional. The gradient of this error functional with respect to density and the Hooke's tensor could be expressed as correlations of an outgoing field with a reconstructed

A two-step approach to depth migration of EM data

misfit field. The reconstructed misfit field was given by a Kirchhoff integral. This makes migration and the first iteration in an inversion procedure identical. Zhdanov and Portniaguine (1997) have shown that a similar system can be obtained for the electromagnetic field using the electromagnetic energy flux density of the misfit field as the error functional,

$$\varepsilon = \int dt \int dS(\boldsymbol{x}_r) n_i \varepsilon_{ijk} \Delta E_j(\boldsymbol{x}_r, t) \Delta H_k(\boldsymbol{x}_r, t), \qquad (1)$$

where n_i is the outward pointing surface normal, ε_{ijk} is the Levi-Civita tensor. The misfit field component $\Delta E_j(\boldsymbol{x}_r, t)$ is the difference between the measured electric field and the electric field predicted by the migration model at the receiver location, $\boldsymbol{x}_r$. The quantity $\Delta H_j(\boldsymbol{x}_r, t)$ is the corresponding magnetic misfit field and $dS(\boldsymbol{x}_r)$ is an infinitesimal receiver surface element. The gradient for conductivity can be expressed as,

$$g_\sigma(\boldsymbol{x}) = \int dt E_m(\boldsymbol{x}, t) \Delta E_m(\boldsymbol{x}, t), \qquad (2)$$

where $E_m(\boldsymbol{x}, t)$ is the outgoing field from the source, calculated in the background migration model,

$$\begin{aligned} E_m(\boldsymbol{x}, t) &= \int dt' \int dV(\boldsymbol{x}_s) \\ & \quad G_{mn}^{EJ}(\boldsymbol{x}, t-t'|\boldsymbol{x}_s, 0) J_n(\boldsymbol{x}_s, t'). \end{aligned} \qquad (3)$$

$G_{mn}^{EJ}(\boldsymbol{x}, t-t'|\boldsymbol{x}_s, 0)$ is the electric Green tensor due to an electric source and $dV(\boldsymbol{x}_s)$ is an infinitesimal source volume element. There is a representation theorem for the reconstructed difference field,

$$\begin{aligned} \Delta E_m(\boldsymbol{x}, t) &= \int dt' \int dS(\boldsymbol{x}_r) n_i \varepsilon_{ijk} \\ & \quad \left[G_{mk}^{EK}(\boldsymbol{x}, 0|\boldsymbol{x}_r, t-t') \Delta E_j(\boldsymbol{x}_r, t') - \right. \\ & \quad \left. G_{mj}^{EJ}(\boldsymbol{x}, 0|\boldsymbol{x}_r, t-t') \Delta H_k(\boldsymbol{x}_r, t') \right]. \end{aligned} \qquad (4)$$

Here $G_{mk}^{EK}(\boldsymbol{x}, 0|\boldsymbol{x}_r, t-t')$ is the adjoint electric Green tensor due to a magnetic source and $G_{mj}^{EJ}(\boldsymbol{x}, 0|\boldsymbol{x}_r, t-t')$ is the adjoint electric Green tensor due to an electric source. The gradient for resistivity is trivially obtained from the conductivity gradient. The first model update can be approximated to be in the negative gradient direction. In the following, the negative of the resistivity gradient is defined as the migrated image. Thus, if the migration results in a positive amplitude value at some location in the image, then a positive resistivity contrast is identified at that location.

Equation 2 is nothing but Claerbouts imaging principle, that is a correlation of an outgoing field with a field reconstructed from recorded boundary conditions. The parameter update in each iteration depends not only on the gradient, but also on the Hessian, which in principle is a non local operator on the gradient. Accounting for the Hessian is a non-trivial task and is not attempted here. The
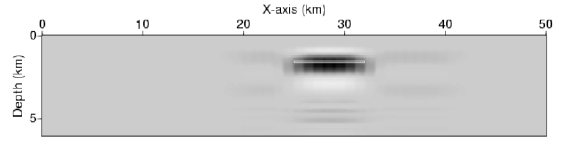

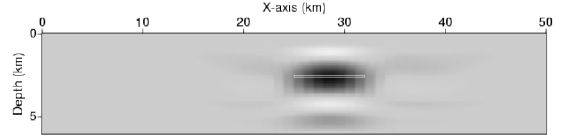Fig. 1: Synthetic data. Shallow reservoir.

Fig. 2: Synthetic data. Deep reservoir.

response from a hydrocarbon filled reservoir has a phase behavior with offset that is consistent with a partially guided or refracted event. The given gradient expression is formally correct but numerical tests have shown that it is not very sensitive to the reservoir depth. Thus, this imaging condition may perform poorly in a one-pass migration scheme. One way around this is to modify the imaging principle to include the effect of laterally propagating energy. Here, this is done by transforming the imaging condition in equation 2 to the frequency domain and introducing a non local operator $\Phi(\boldsymbol{x}|\boldsymbol{x}', \omega)$,

$$I_\rho(\boldsymbol{x}) = \int dV(\boldsymbol{x}') \int d\omega \Phi(\boldsymbol{x}|\boldsymbol{x}', \omega) E_m(\boldsymbol{x}, \omega) \Delta E_m^*(\boldsymbol{x}', \omega) \quad (5)$$

$I_\rho(\boldsymbol{x})$ is the image with respect to resistivity contrasts.

It turns out that a simplified model can explain the main features of the SBL data for intermediate and large source receiver separations. We assume that the field propagate from the source down to the reservoir with a down going Green function, couples with a laterally propagating Green function in the reservoir which again couples with an upgoing Green function that take the response to the receiver. Thus, EM data with small source-receiver offsets are not used in this migration scheme. The laterally propagating Green function, $\Gamma(\boldsymbol{x} - \boldsymbol{x}', \omega)$, can be estimated with a plane layer modeling algorithm where the Green function is excited and recorded at reservoir depth. Thus,

$$\Phi(\boldsymbol{x}|\boldsymbol{x}', \omega) = \Phi(\boldsymbol{x} - \boldsymbol{x}', \omega) = \lambda \Gamma(\boldsymbol{x} - \boldsymbol{x}', \omega), \qquad (6)$$

where λ is a (complex) coupling factor describing the field coupling in to, and out of, the thin high resistive layer. The operator $\Phi(\boldsymbol{x} - \boldsymbol{x}', \omega)$ depend on the resistivity, σ_r, and thickness, h_r, of an assumed resistivity anomaly. For a given set of σ_r and h_r, the width and depth of the anomaly will be determined by the migration scheme. Migration is performed by transforming equation 3 and equation 4 to the frequency domain and applying the imaging condition in equation 5. Both phase and ampli-

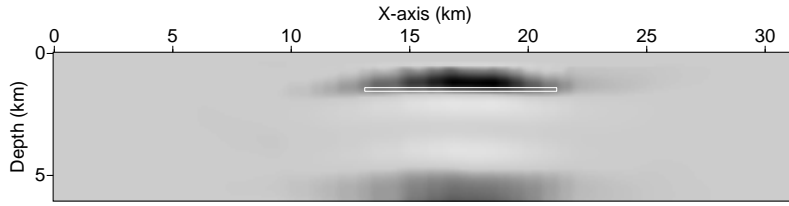# A two-step approach to depth migration of EM data

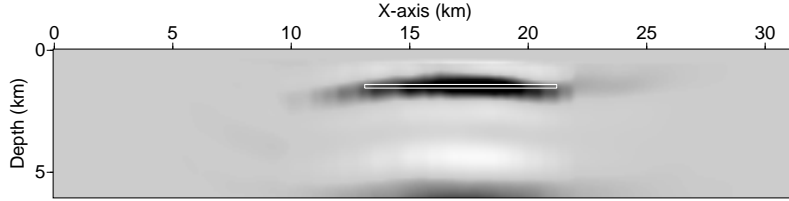Fig. 3: Real data. Both anomaly magnitude and thickness assumed small.

Fig. 4: Real data. Both anomaly magnitude and thickness from best fit model.

tude for the source current and the recorded EM data are used in the migration. Only phases for the Green functions are used. The total phase of the outgoing field from source to image location include the laterally propagating energy. The parameters σ_r and/or h_r may in principle be unknown. These parameters are estimated by a limited set of forward modeling operations. Based on our experience up to present, we make the assumption that the lateral distance and width of the anomaly is given by the first migration step. Several resistivity models that include a reservoir are generated. The migration resistivity model is used as a basis. Reservoirs that vary in magnitude, thickness and depth are added to the basis model. A forward finite-difference simulation is performed for each of these models. The difference between the real data and the synthetic datasets is calculated in each case. The difference data with smallest errors point to the most probable models. A final remigration with the most probable σ_r and h_r values is performed. The migrated depth and the most probable depth from the forward modeling is then compared. An inconsistency may point to an error in the background resistivity model.

Results

Figure 1 and Figure 2 show results from depth migration of synthetic data. For the example in Figure 1, the true reservoir depth is 1500 m and for the example in Figure 2 the true reservoir depth is 2500 m. The reservoir locations are marked with white rectangles. The water depth is 500 m, but the effect of the air wave is not included in the synthetic data. It is assumed that proper up down separation is performed as a preprocessing step before the depth migration. For both cases the reservoir has a resistivity of 60 Ωm and the formation has a resistivity of 2.5 Ωm. In these images, black indicates increased resistivity compared to the background migration resistivity model. Data with equally spaced frequencies from 0.25 Hz to 2 Hz with a step of 0.25 Hz is used to create the images. Laterally, the reservoir seems to be well defined in both cases. Due to the limited number of frequencies we must expect side lobes to the reservoir image with depth or in some cases even replication of the reservoir image with depth. The effect does not seem to be too severe here. In both cases, the reservoir is slightly overmigrated, however, the method is clearly sensitive to true reservoir depth. For the synthetics, both reservoir thickness and magnitude is known. A second step to determine these parameters is not required.

Figure 3 and Figure 4 show migration of data acquired over the Troll field. The water depth is here 320 m and the air wave has a large effect on the data. In this case it is essential to separate in up and downgoing components of the EM field before depth migration. Up down separation requires that both electric and magnetic fields are recorded at each receiver station. After up down separation, the airwave appears in the downgoing component only. It is the upgoing component that is used as boundary condition in the migration. If up down separation is not performed, then the airwave will image falsely as high resistivity in the formation. The background resistivity model was determined from forward modeling tests and plane layer inversion, matching data outside the known reservoir area. In this way it is ensured that the background migration model explains the main trends in the data when both source and receiver are far from the reser-

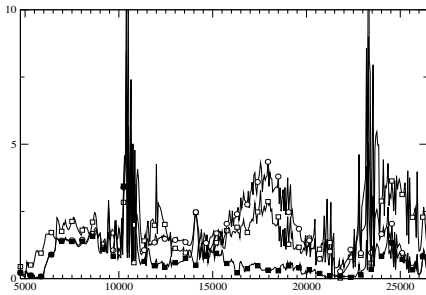**A two-step approach to depth migration of EM data**

Fig. 5: Distribution of misfit along tow line.

voir.

For the migration, frequencies of 0.25 Hz, 0.75 Hz and 1.25 Hz were used. Figure 3 show the result of depth migration, assuming $\sigma_r = 100$ Ωm and $h_r = 20$ m. The known reservoir location is marked with a white rectangle. It is obvious that the reservoir is undermigrated in this case. The average migrated depth is approximately 1100 m as compared to the known depth interval of 1400 m to 1550 m. A series of forward modeling operations was performed. Examples of the error distribution along the tow line for 3 of these models are shown in Figure 5. The lowest error is for a model with $\sigma_r = 100$ Ωm, $h_r = 100$ m and a depth to top reservoir of 1400 m. This line is marked with black squares. The two other lines in Figure 5 are for models with larger errors. The line marked with open squares is for a model that have $\sigma_r = 100$ Ωm, $h_r = 20$ m and a depth to top reservoir of 1400 m. The line marked with open circles is for a model that have $\sigma_r = 100$ Ωm, $h_r = 100$ m and a depth to top reservoir of 1800 m. The full set of difference data for all the forward modeling operations give a probability distribution that peak for a reservoir with thickness between 100 m and 200 m and magnitude between 100 Ωm and 200 Ωm. All these models give similar total errors and similar migrated images. One example is shown in Figure 4. This migration is done with $\sigma_r = 100$ Ωm and $h_r = 100$ m.

The lateral resolution is acceptable with the highest amplitudes at the known reservoir location. The vertical resolution seems even better than for synthetics. One reason for this may be that the background resistivity model is approximately 1 Ωm above and below the reservoir depth. Thus, locally higher spatial wavenumbers in the migrated EM field, as compared to the synthetic case, might increase resolution in depth.

Conclusion

In order to migrate EM data from a low frequency controlled source, proper 3D electromagnetic Green functions should be used since the near-field effects may be large. Imaging principles of the correlation type do not have sufficient depth sensitivity to be used in an one-pass

migration step. Depth sensitivity is increased if a non local operator is introduced in the imaging condition. This operator account for the lateral propagation of the EM field in the high resistivity reservoir. The cost of introducing this new operator is that two new parameters must be determined. To do this, a second step in the migration process have been introduced. This step consists of forward modeling operations. A suite of models based on the migration resistivity model is generated. All these model have a high resistivity anomaly, where the lateral extent of the anomaly is taken from the first migration step. Based on the error distributions obtained from the difference between the synthetic and real data, a final migration is performed with the parameter sets that give the best fit between real and synthetic data.

References

Eidesmo, T., Ellingsrud, S., MacGregor, L.M., Constable, S., Sinha, M.C., Johansen, S., and Kong, F.N., 2002, Sea bed logging (sbl), a new method for remote and direct identification of hydrocarbon filled layers in deepwater areas:: First Break, **20**, 144–152.

Mittet, R., Amundsen, L., and Arntsen, B., 1994, Iterative inversion/migration with complete boundary conditions for the residual misfit field:: J. Seis. Expl., **3**, 141–156.

Mittet, R., Sollie, R., and Hokstad, K., 1995, Prestack depth migration with compensation for absorbtion and dispersion: Geophysics, **60**, 1485–1494.

Tompkins M.J., 2004, Marine controlled-source electromagnetic imaging for hydrocarbon exploration:interpreting subsurface electrical properties:: First Break, **22**, 45–51.

Zhdanov, M.S., and Portniaguine, O., 1997, Time-domain electromagnetic migration in the solution of inverse problems:: Geophys. J. Int., **131**, 293–309.